PAPER

Check for updates

LiCoO$_2$ impregnated nano-hierarchical ZSM-5 assisted catalytic upgrading of Kraft lignin-derived liquefaction bio-oil†

Ashutosh Agarwal [iD] *[a,b] and Xue Li*[c]

In this study, Kraft lignin-derived bio-oil was upgraded with LiCoO$_2$ or Co$_3$O$_4$-impregnated hierarchical nano-ZSM-5 catalysts. The synthesized catalysts were characterized by N$_2$-Ads-Des, XRD, XPS, NH$_3$-TPD, FTIR, FESEM and ICP-OES analyses. Upon incorporation of LiCoO$_2$ and Co$_3$O$_4$ onto the HZSM-5 support, the MFI structure of HZSM-5 remained intact. All the catalysts displayed a combination of Type-I and -IV isotherms. The upgraded bio-oil showed a significant increase in the amounts of alkylated guaiacols owing to the reduction in unsubstituted guaiacols, alkenyl guaiacols, and homovanillic acid. Hydrogenation, alkylation, and deoxygenation were the plausible bio-oil upgrading pathways. With the increase in cobalt content, weak acidity decreased through all the catalysts, while LiCoO$_2$ provided supplementary acid sites that increased the total acidity of LiCoO$_2$/HZSM-5 compared to the Co$_3$O$_4$/HZSM-5 catalyst. LiCoO$_2$/HZSM-5 with a low cobalt content (5% and 10% Co) displayed high selectivity for the production of alkylated guaiacols owing to their strong acidity. The upgraded bio-oils showed an increase in carbon and hydrogen followed by a decrease in oxygen content. The maximum higher heating value (~29.83 MJ kg^{-1}) was obtained for the 10% Co (LiCoO$_2$)/HZSM-5 catalyst. In general, LiCoO$_2$/HZSM-5 outperformed the Co$_3$O$_4$/HZSM-5 catalyst. XRD of the spent 10% Co (LiCoO$_2$)/HZSM-5 suggested the complete loss of lithium from the catalyst with the retention of the MFI structure of the HZSM-5 support. In this study, it was successfully demonstrated that the main constituent of the cathode material of spent lithium-ion batteries *i.e.* LiCoO$_2$ could be employed to synthesize a novel and cheap catalyst for bio-oil upgrading while addressing the e-waste management issue in a sustainable manner.

1. Introduction

Increasing concerns about energy and environmental sustainability amid depleting fossil fuels and increasing global warming have prompted a need for the exploration of renewable energy resources.[1–3] Replacing fossil fuels with upgraded bio-oils obtained *via* depolymerization of biomass is an appealing alternative to reduce the massive consumption of fossil fuels.[4] In nature, lignin is one of the richest resources of renewable aromatic hydrocarbons.[5] Among various kinds of

lignin, Kraft lignin is the most recalcitrant lignin that has acquired the highest total addressable global market of more than 40 Mton per year.[6] Thermochemical liquefaction of Kraft lignin for the production of high-quality bio-oil by employing supercritical fluids has recently gained significant attention. The bio-oil obtained *via* this process must be upgraded before employing it as transportation fuel owing to its high oxygen content, low heating value, immiscibility with conventional fuels, and chemical/thermal instability.[7,8] Catalysts play a vital role in influencing the cost and quality of upgraded bio-oil and hence the choice of catalysts becomes highly crucial. During the past decade, several heterogeneous catalysts involving noble metals, transition metals, metal sulfides, metal nitrides, *etc.* incorporated on acidic supports such as Al$_2$O$_3$ and zeolites have been investigated for bio-oil production and upgrading.[9–13] Lately, non-noble transition metals *viz.* nickel, zinc, molybdenum, and cobalt have also received special focus due to their immense potential for deep deoxygenation with minimum hydrogen consumption and carbon loss.[14–18] For instance, fast pyrolysis of lignin over cobalt oxide embedded on HZSM-5 provided it with decent catalytic behavior for direct

[a]*Department of Environment and Energy Engineering, Chonnam National University, Gwangju 61186, Republic of Korea*
[b]*Engineering Product Development, Singapore University of Technology and Design, 8 Somapah Road, 487372, Singapore. E-mail: ashutosh_agarwal@sutd.edu.sg*
[c]*Department of Materials Science and Engineering, Luoyang Institute of Science and Technology, Louyang, 471023, P.R. China. E-mail: lixue0377@lit.edu.cn*
†Electronic supplementary information (ESI) available: Schematic illustration of the experimental procedure; FTIR absorption spectra of all the synthesized Co$_3$O$_4$/HZSM-5 and LiCoO$_2$/HZSM-5 catalysts; actual metal contents of all the synthesized LiCoO$_2$ and Co$_3$O$_4$ loaded HZSM-5 catalysts. See DOI: https://doi.org/10.1039/d4nr00358f

View Article Online

Nanoscale

deoxygenation of lignin.[19] Besides, cobalt nitride supported on nitrogen-doped carbon has been quite promising for hydrodeoxygenation (HDO) of lignin-derived phenols under mild conditions. Over this catalyst, a maximum yield of more than 99.9% was obtained upon HDO of eugenol to propylcyclohexanol.[20] Catalysts composed of cobalt phosphide (Co_xP_y) have also shown excellent catalytic activity for HDO of phenol and dibenzofuran.[21] In addition, HDO of cyclohexanone over an alumina-supported cobalt–molybdenum catalyst has been found to favor more than 89% cyclohexanone conversion with 100% hydrocarbon selectivity.[16] More recently, Ni–Co/γ-Al_2O_3 catalysts prepared via the co-precipitation method were found to promote the formation of the $NiCo_2O_4$ spinel structure with specific active sites for direct deoxygenation/demethoxylation of guaiacol.[22] This resulted in 98.9% guaiacol conversion with 59.1% and 35.2% cyclohexane and benzene selectivities, respectively. Although several cobalt-based catalysts have demonstrated decent catalytic activity for bio-oil upgrading, these catalysts have remained unpreferred due to their high cost and economic inefficiency. Hence, there is an urgent need to develop economically viable green catalysts for bio-oil upgrading.

"Waste-to-wealth" is one of the prominent pillars of sustainable green chemistry research. In this direction, numerous industrial solid waste catalysts containing metal oxides have been recently employed to enrich the quality of bio-oil. These catalysts effectively improved the calorific value of bio-oil while reducing its oxygen content, acidity, and viscosity.[23] However, "waste-to-wealth" sustainable management of electronic waste (e-waste) remains a major challenge for the scientific community. Spent Li-ion batteries (LIBs) form the major portion of e-waste. It has been estimated that in the next two decades spent LIBs from electric vehicles will build up to anywhere between 0.33 and 4 million tons of e-waste worldwide.[24] Since the landfill disposal of spent LIBs poses a serious risk to the surrounding environment, it is highly crucial to recycle or reuse this waste for a better cause. Spent LIBs are a huge source of numerous metal oxide-based catalysts. Catalysts recovered from spent LIBs have found applications in electro- and photo-catalytic water splitting,[25] organic pollutant degradation[26] and biomass pyrolysis/gasification.[27,28] For instance, Co_3O_4 obtained from a spent $LiCoO_2$ battery was found to be highly efficient in the total oxidation of volatile organic compounds. Very recently, the products obtained upon thermal treatment of spent $LiCoO_2$ batteries have shown substantial activity in upgrading biomass pyrolysis products by significantly promoting catalytic cracking (i.e. H-transfer) of lignin-derived phenols to hydrocarbons and aliphatics.[27,29,30] However, the solvothermal catalytic upgrading of liquefaction bio-oil by employing the $LiCoO_2$ catalyst remains unknown. Following the concept of "waste to wealth" sustainable management of e-waste and to further encourage spent LIB-based catalysts' application, the main constituent of the cathode material of spent LIBs i.e. $LiCoO_2$ was chosen for the first time in this research for upgrading of bio-oil by employing a solvothermal process. The schematic illustration of the experi-

mental procedure is shown in Fig. S1 (ESI†). For comparison, catalysts for bio-oil upgrading were synthesized by incorporating varying concentrations of $LiCoO_2$ and Co_3O_4 over a hierarchical nano-ZSM-5 support. The synthesized catalysts were characterized by several analytical methods such as nitrogen adsorption–desorption (Ads–Des) analysis, X-ray photoelectron spectroscopy (XPS), X-ray diffraction (XRD), ammonia-temperature programmed desorption (NH_3-TPD), Fourier transform infrared (FTIR) spectroscopy, field emission scanning electron microscopy (FESEM) and inductively coupled plasma-optical emission spectroscopy (ICP-OES). After upgrading, the upgraded bio-oils were analyzed by carbon, hydrogen, nitrogen, and sulfur (CHNS) elemental analysis and the gas chromatography-mass spectrometry (GC-MS) technique. Finally, the best-spent catalyst was characterized by XRD, ICP-OES, and thermogravimetric (TG) analysis. Hierarchical nano-ZSM-5 was selected as the support material for $LiCoO_2$ and Co_3O_4 due to its high thermal stability and shape selectivity. Additionally, the mesopores present in hierarchical nano-ZSM-5 were utilized to enable easy diffusion of molecules to the acid sites for HDO and alkylation of reactant molecules.[31]

2. Materials and methods

2.1 Materials

Kraft lignin, $LiCoO_2$ (99.8%), $Co(OAc)_2\cdot4H_2O$ (99.999%), acetone (≥99.9%), ethanol (≥99.8%), ammonium nitrate (≥99%), aluminum isopropoxide (AIP, ≥98%) and tetraethyl orthosilicate (TEOS, 98%) were purchased from Sigma-Aldrich. Forty percent aqueous solution of tetrapropylammonium hydroxide (TPAOH) was acquired from Merck. High-purity hydrogen and nitrogen gases (≥99%) were procured from Daedeok Gas Co. Ltd (South Korea). As the stoichiometric ratio of lithium and cobalt in $LiCoO_2$ obtained from the cathode material of spent LIBs does not differ considerably from the standard $LiCoO_2$ nanoparticles, the latter were employed in this study considering the repeatability of the experiments.[32,33] $LiCoO_2$ nanoparticles can however be obtained from the cathode material of spent LIBs by following the procedure as described elsewhere.[32,33]

2.2 Synthesis of $LiCoO_2$ and Co_3O_4 impregnated hierarchical nano-ZSM-5

The molar composition ratio $3TPAOH:0.5Na_2O:0.5Al_2O_3:25SiO_2:450H_2O$ was used to synthesize nano hierarchical ZSM-5 crystals following the procedure as specified elsewhere.[34] In this study, a SiO_2/Al_2O_3 ratio of 25:0.5 was used to obtain uniform mesoporous single crystals and to minimize coke formation during catalytic activity.[34] Briefly, AIP was mixed for 2 h with a solution of TPAOH and NaOH at 25 °C to attain a clear aluminate solution. It was then added slowly to TEOS and shaken at 25 °C for 24 h to completely hydrolyze TEOS followed by hydrothermal treatment in an autoclave (Teflon-lined) at 165 °C for 27 h. After hydrothermal treatment, the white crystals formed were separated via cen-

This journal is © The Royal Society of Chemistry 2024

trifugation at 14 000 rpm. Subsequently, they were dried overnight at 100 °C and calcined (550 °C, 5 °C min^{-1}, 6 h) in static air. The crystals were then refluxed for 24 h with 0.8 M NH$_4$NO$_3$ (150 mL) at 80 °C and the protonated crystals thus obtained were again dried overnight at 100 °C. Finally, the crystals were calcined (550 °C, 5 °C min^{-1}, 5 h) in static air.

Different mass ratios of LiCoO$_2$ and Co(OAc)$_2$·4H$_2$O containing 5, 10, and 20% cobalt were incorporated into the synthesized nano-hierarchical ZSM-5 support *via* an ultrasound-assisted wet impregnation method. Briefly, the reaction mixture was first subjected to 40 kHz ultrasound at 50% duty cycle for 15 min and then left untouched for 3 h at 25 °C. After impregnation, the catalysts were dried for 10 h at 120 °C followed by calcination (550 °C, 5 °C min^{-1}, 5 h) in static air. This resulted in the decomposition of Co(OAc)$_2$·4H$_2$O to Co$_3$O$_4$. All the catalysts were finely ground with a mortar and pestle. After grinding, they were sieved with a 100-mesh sieve. The catalysts were labeled as 5% Co (LiCoO$_2$)/HZSM-5, 10% Co (LiCoO$_2$)/HZSM-5, 20% Co (LiCoO$_2$)/HZSM-5, 5% Co (Co$_3$O$_4$)/HZSM-5, 10% Co (Co$_3$O$_4$)/HZSM-5 and 20% Co (Co$_3$O$_4$)/HZSM-5 according to the weight percentage of Co loading.

2.3 Catalyst characterization

Nitrogen Ads-Des isotherms were recorded at −196 °C using a BELCAT-A instrument. Before recording the isotherms, the catalysts were subjected to 10^{-6} Torr vacuum at 150 °C for 3 h to remove any moisture. The specific surface area of the catalysts was evaluated by the Brunauer–Emmett–Teller (BET) method. The microporous and mesoporous volumes were determined by the t-plot method while the pore size distribution of mesopores (>3 nm) and micropores (<2 nm) were obtained by the Barrett–Joyner–Halenda (BJH) method and micropore analysis methods, respectively. A relative pressure of P/P_o = 0.990 was used to evaluate the total pore volume.

Powder XRD patterns were acquired over a 3D PANalytical EMPYREAN high-resolution X-ray diffractometer. This diffractometer was equipped with a PIXEL 3D Medipix 3 Bragg–Brentano detector. Monochromatic Cu Kα radiation (λ = 1.5406 Å) operated at 40 kV and 40 mA was used to irradiate the samples. A scanning rate of 0.417° min^{-1} was applied to record the data within a 2θ range from 5° to 90° and at a step size of 0.02°. The quantitative analysis was not performed with the XRD patterns. eqn (1) (Scherrer's formula) was used to estimate the crystal size at the prominent peak positions. The average crystallite size was evaluated by calculating the mean of all the obtained crystal sizes.

$$\tau = \frac{K\lambda}{\beta \cos \theta} \qquad (1)$$

where τ, θ, β, K, and λ denote the crystal size (nm), Bragg's angle (°), full width at half maxima (radians), shape factor (0.9) and wavelength (1.5406 Å), respectively.

The acid site density of the catalysts was determined by NH$_3$-TPD. A BELCAT-B temperature programming unit installed with a mass spectrometer and a thermal conductivity detector was used to record the NH$_3$-TPD curves. Before analysis, the catalysts were subjected to H$_2$/He and then treated with 5% NH$_3$/He gas for 1 h at 100 °C. The NH$_3$-TPD profile was acquired within a temperature range of 100–800 °C.

A Spectrum 400 FTIR spectrometer (PerkinElmer, USA) was used to record the FTIR absorption spectra. All the spectra were recorded at an effective resolution of 4 cm^{-1} with 32 scans each. The FTIR samples were prepared by grinding the catalysts with KBr in a mass ratio of 1 : 150. Li and Co contents of the synthesized catalysts were estimated by using an Optima 8300 ICP-OES (PerkinElmer, USA).

FESEM images were obtained at a magnification of 20 KX and EHT = 15 kV over a JSM-7500F scanning electron microscope (JEOL USA). Before FESEM imaging, the secondary electron signal necessary for topographic examination was improved by sputter-coating the catalysts with platinum (Pt). A PerkinElmer PHI-1600 X-ray photoelectron spectrometer was used to record the XPS spectra using Mg Kα (1253.6 eV) monochromatic irradiation.

The thermal degradation behavior of fresh and spent catalysts was analyzed using a TG analyzer (DTG-60H, Shimadzu, Japan). For each analysis, nearly 10 mg of the catalyst was placed in a platinum crucible and heated under an N$_2$ atmosphere (99.999%) up to 900 °C. The heating rate was set at 10 °C min^{-1}. Throughout the analysis, the flow rate of N$_2$ was maintained at 50 mL min^{-1}.

2.4 Production and upgrading of stock bio-oil

Kraft lignin was solvothermally depolymerized in a 300 mL Hastelloy-C-276 HR-8300 batch reactor to produce the stock bio-oil. The reactor was equipped with a Parr 4848 controller. Briefly, the reaction mixture was formulated by mixing Kraft lignin (20 g) with ethanol (200 mL). The mixture was placed in the reactor and an inert atmosphere of 1 MPa high-purity N$_2$ was developed in the reactor. The reactor was then heated to 300 °C. At this stage, the pressure inside the reactor reached up to 10 MPa. The temperature inside the reactor was maintained at 300 °C for 1 h and the reaction mixture was constantly stirred at a speed of 250 rpm. At the end of the reaction, an ice-water bath was used to instantaneously cool down the reactor. The bio-oil was solubilized in excess of ethanol and then filtered to get rid of coke and unreacted lignin. Finally, the stock bio-oil was subjected to rotary evaporation at 55 °C under reduced pressure to remove ethanol.

For bio-oil upgrading, stock bio-oil (3 g) was dissolved in ethanol (50 mL) in a 150 mL batch reactor. To this, a 300 mg catalyst was added and mixed thoroughly. Hydrogen was purged in this mixture and a pressure of 1 MPa was created in the reactor. It was then heated up to 300 °C and the temperature was maintained for 1 h. The pressure inside the reactor reached up to 8 MPa. During the entire process, the reaction mixture was stirred constantly at a speed of 250 rpm. At the end of the reaction, an ice-water bath was used to instantaneously cool down the reactor. The upgraded bio-oil was then separated by filtration. Excess ethanol was used to wash the catalyst to extract upgraded bio-oil. In the end, tar was

removed by washing the catalysts with acetone. The catalysts were then dried at 110 °C. Finally, the upgraded bio-oils were subjected to rotary evaporation under reduced pressure at 55 °C to remove ethanol. GC-MS and CHNS analysis were performed to characterize the upgraded bio-oil samples. All the bio-oil upgrading experiments were performed thrice and each data represents the mean of triplicate experiments. The experimental data were within the limits of 1SD from the mean.

2.5 Characterization of bio-oil

A GC-MS system (Agilent 6890) was employed to determine the chemical compositions of both the stock and upgraded bio-oil samples. The GC-MS system was installed with an HP-5 MS column. The sample preparation was carried out by diluting the upgraded bio-oil with high-performance liquid chromatography (HPLC) grade ethanol. The injection temperature and volume were fixed at 280 °C and 1 μL, respectively. Helium was used as the carrier gas at a flow rate of 1 mL min^{-1}. The heating rate and the initial oven temperature were fixed at 5 °C min^{-1} and 40 °C, respectively. Two ramps with 2 min hold time each were set at 170 °C and 300 °C.

A Vario MACRO cube/elemental (Germany) CHNS analyzer was used to determine the elemental compositions of the stock and upgraded bio-oils. Boie's formula eqn (2) was applied to estimate the higher heating values (HHV) based on the elemental percentages of carbon, hydrogen, nitrogen, oxygen, and sulfur.[35]

$$\text{HHV}_{\text{Boie}}(\text{MJ kg}^{-1}) = 0.3516\,\text{C} + 1.1622\,\text{H} - 0.1109\,\text{O} + 0.0628\,\text{N} + 0.1046\,\text{S} \quad (2)$$

2.6 Spent catalyst characterization and stability

TG analysis was used to estimate the quantity of coke deposited on the best-spent catalyst. The possible structural changes and metal leaching in the spent catalyst were evaluated by XRD and ICP-OES analysis, respectively. Before XRD and ICP-OES, the coke deposited on the spent catalyst was removed by calcination (550 °C, 5 °C min^{-1}, 5 h) in static air.

3. Results and discussion

3.1 Characterization of catalysts

3.1.1 XRD analysis. The powder XRD patterns of LiCoO$_2$ and Co$_3$O$_4$ loaded HZSM-5 catalysts are shown in Fig. 1a and b, respectively. A doublet and a triplet between $2\theta = 7°–10°$ and 22°–25°, respectively which represent the mordenite framework inverted (MFI) characteristic structures of HZSM-5 are visible in the XRD patterns of all the synthesized catalysts. This suggests that the MFI structure of HZSM-5 remained
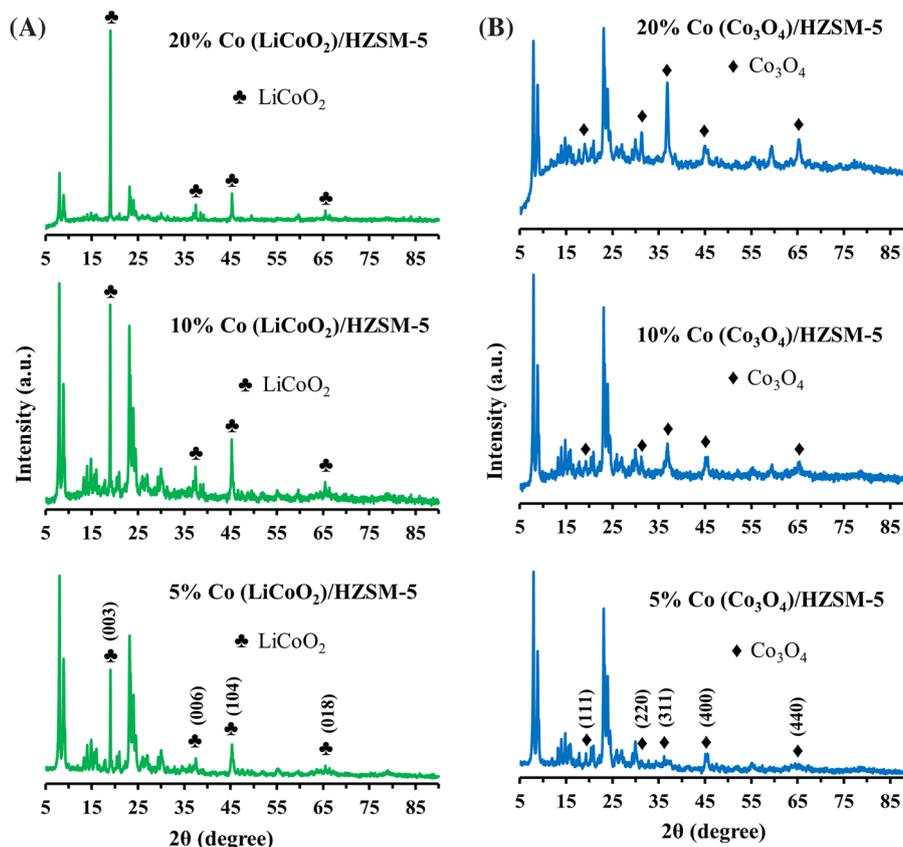

Fig. 1 (a) XRD patterns of 5%–20% Co(LiCoO$_2$)/HZSM-5 catalysts. (b) XRD patterns of 5%–20% Co(Co$_3$O$_4$)/HZSM-5 catalysts.

intact even after the incorporation of $LiCoO_2$ and Co_3O_4 onto the HZSM-5 support. All the $LiCoO_2$ loaded HZSM-5 catalysts showed diffraction peaks at 2θ = 18.9°, 37.4°, 45.0°, 64.0° corresponding to the (003), (006), (104) and (018) crystal planes of $LiCoO_2$, respectively (JCPDS no. 44-145) (Fig. 1a). The strong diffraction peak at 18.99° and the medium intensity peaks at 37.44° and 45.00° indicate the existence of a rhombohedral unit cell ($R3m$ space group).[36] This confirms that $LiCoO_2$ remained undecomposed even after calcination at 550 °C owing to its thermally stable structure.[37] The XRD patterns of Co_3O_4 loaded HZSM-5 catalysts showed diffraction peaks at 2θ = 19.0°, 31.3°, 36.5°, 44.8°, 65.2° corresponding to the (111), (220), (311), (400) and (440) crystal planes of Co_3O_4, respectively (JCPDS no. 80-1545) (Fig. 1b). The appearance of a strong diffraction peak at 2θ = 36.5° confirms the formation of Co_3O_4. From the XRD patterns, it is evident that the prominent peaks at 2θ = 18.9° and 45° (Fig. 1a) corresponding to the (003) and (104) crystal planes of $LiCoO_2$ and the peaks at 2θ = 36.5° and 65.2° (Fig. 1b) corresponding to the (311) and (440) crystal planes of Co_3O_4 showed a significant increase in the peak intensity with the increase in the mass percentage loading of Co. It was found that the increase in diffraction peak intensities for Co_3O_4 did not follow the same trend as that of $LiCoO_2$. In addition, with the increase in Co content, the XRD pattern of Co_3O_4-loaded HZSM-5 catalysts showed more obvious background signals. This was because Co_3O_4 was obtained upon the decomposition of $Co(OAc)_2 \cdot 4H_2O$ while $LiCoO_2$ remained undecomposed during the calcination process. Consequently, the crystal growth patterns of the two compounds were significantly different which is apparent from the FESEM images.

3.1.2 BET analysis. Fig. 2 shows the nitrogen Ads-Des isotherms and the pore size distributions of all the synthesized $LiCoO_2$ and Co_3O_4 loaded HZSM-5 catalysts. According to the International Union of Pure and Applied Chemistry (IUPAC) classification, all the catalysts displayed a combination of Type-I and -IV isotherms (Fig. 2C). The Type-I isotherm was characterized by the existence of a plateau and the absence of a hysteresis loop at relatively low pressure while the presence of a hysteresis loop at relatively high pressure suggested a Type-IV isotherm.[38] The hysteresis loop at relatively high pressure was associated with the capillary condensation inside the mesopores. The formation of a hierarchical porous system with micropores and mesopores was evident by the coexistence of Type-I and -IV isotherms. For all the catalysts, the micropore and mesopore size distributions ranged from <1.5 nm and 2–100 nm, respectively (Fig. 2A and B) with a certain degree of similarity within the respective pore size distributions. Table 1 lists the surface areas and pore volumes as calculated from the nitrogen Ads-Des isotherms. In Table 1, the BET surface area (S_{BET}) denotes the aggregate of the contributions of the Ads-isotherms from both the external and the internal surfaces. A decrease in total pore volume and BET surface area with an increase in the percentage content of cobalt suggests the deposition of $LiCoO_2$ and Co_3O_4 in the pores and channels of the HZSM-5 support.

3.1.3 XPS analysis. The XPS spectra of the 1s shell of oxygen and 2p subshells of aluminum, silicon, and cobalt for 10% Co ($LiCoO_2$)/HZSM-5 and 5% Co (Co_3O_4)/HZSM-5 catalysts are shown in Fig. 3. The peak corresponding to Li (1s) was not taken into account due to its very low sensitivity. The oxidation
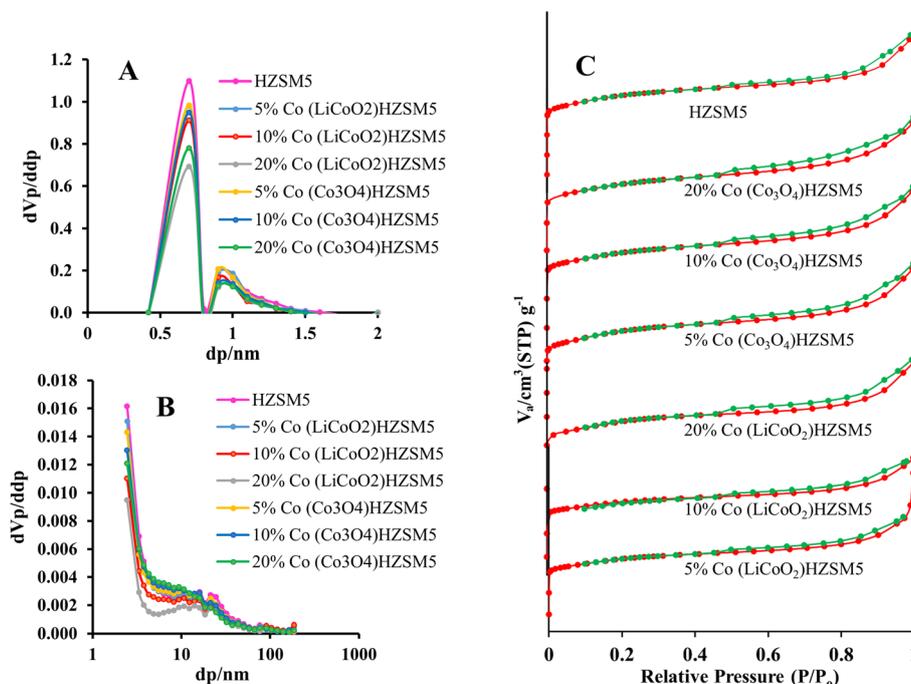
Fig. 2 N$_2$ Ads/Des isotherms (C) and pore size distributions (micropores (A) and mesopores (B)) of all the synthesized $LiCoO_2$ and Co_3O_4 loaded HZSM-5 catalysts.

**Table 1** Textural properties of all the synthesized LiCoO$_2$ and Co$_3$O$_4$ loaded HZSM-5 catalysts

	S_{BET} (m^2 g^{-1})	Pore volume (cm^3 g^{-1}) Total	Average crystallite size (nm)		
			mesopores	Micropores	
HZSM5	417	0.31	0.16	0.15	35.7
5% Co (LiCoO$_2$)/ HZSM5	362	0.27	0.15	0.12	41.1
10% Co (LiCoO$_2$)/ HZSM5	324	0.25	0.14	0.11	44.4
20% Co (LiCoO$_2$)/ HZSM5	248	0.18	0.09	0.09	133.8
5% Co (Co$_3$O$_4$)/ HZSM5	372	0.27	0.14	0.13	33.5
10% Co (Co$_3$O$_4$)/ HZSM5	345	0.26	0.14	0.12	23.6
20% Co (Co$_3$O$_4$)/ HZSM5	295	0.23	0.13	0.10	11.5

state of cobalt was determined by the binding energy spin–orbit component. The XPS spectrum of cobalt was split into two components *i.e.* 2p$_{3/2}$ and 2p$_{1/2}$ with an intensity ratio of 2 : 1 (Fig. 3D and E). In the cobalt 2p XPS spectra, the peaks located at 796.17, 797.55 and 780.85, 781.51 eV were ascribed to the spin–orbital peaks of Co 2p$_{1/2}$ and Co 2p$_{3/2}$, respectively. Each component was denoted by a main spectral line and a satellite peak. Since Co$_3$O$_4$ is an oxide of the mixed oxidation state of cobalt, the presence of satellite features due to the +2 and +3 oxidation states of cobalt in Fig. 3E confirmed the presence of Co$_3$O$_4$. The prominent satellite peaks of cobalt in

Fig. 3D were interpreted by the molecular orbital theory.[39] As per the electronic ground state configuration of LiCoO$_2$ *i.e.* 2p^6 3d^6 L, six electrons fill the 3d-shell of cobalt while the other six electrons fill the 2p-shell of oxygen (the ligand shell L). Upon excitation, one electron jumps from ligand shell L to the metal 3d-shell, and the main spectral line is denoted by the configuration 2p^5 3d^7 L^{-1}. The satellite peak is a consequence of the ligand-to-metal shakeup charge transfer which is assigned to the configurations 2p^5 3d^6 L and 2p^5 3d^8 L^{-2}. Here the intensity of these peaks depends on both the environment and the oxidation state of the metal. In Fig. 3A, B, and C, the binding energies of aluminum (2p), silicon (2p), and oxygen (1s) at 75.68, 104.08 and 532.38 to 533.88 eV, respectively, were consistent with that of Al$_2$O$_3$ (532.38 eV for O 1s) and SiO$_2$ (533.88 eV for O 1s) that mold the HZSM-5.

3.1.4 NH$_3$-TPD analysis. The NH$_3$-TPD spectra of all the synthesized catalysts are shown in Fig. 4A and B. The two desorption peaks at <300 °C and >525 °C represent weak and strong acid sites, respectively.[40] Usually, the maximum peak temperature denotes the acidity of sites while the peak areas represent the relative concentration of strong and weak acid sites.[41] The number of acid sites concerning strong and weak acid sites as expressed in mmol NH$_3$ g^{-1} catalyst are mentioned in Table 2. With the increase in cobalt content, weak acidity decreased for all the catalysts while strong acidity increased only for the LiCoO$_2$/HZSM-5 catalysts due to a proportional increase in lithium content. The loading of LiCoO$_2$ provided supplementary acid sites that increased the total
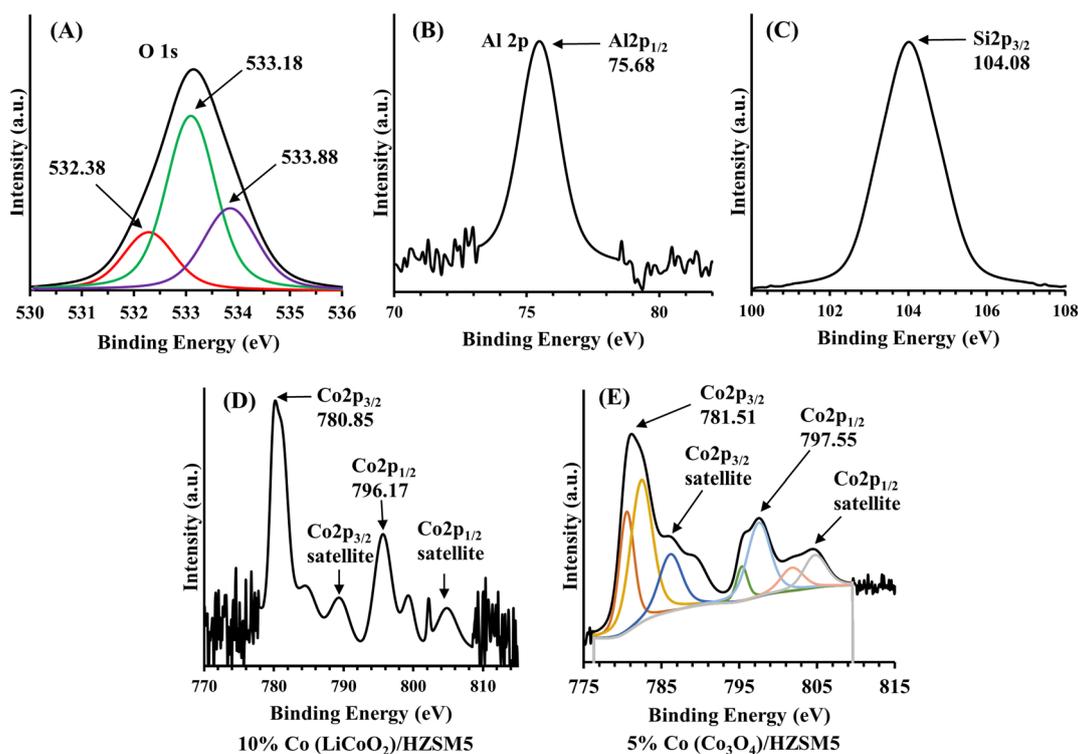
Fig. 3 XPS spectrum of (A) O (1s), (B) Al (2p), (C) Si (2p), (D) Co (2p) of 10% Co (LiCoO$_2$)/HZSM-5 and (E) Co (2p) of the 5% Co (Co$_3$O$_4$)/HZSM-5 catalyst.
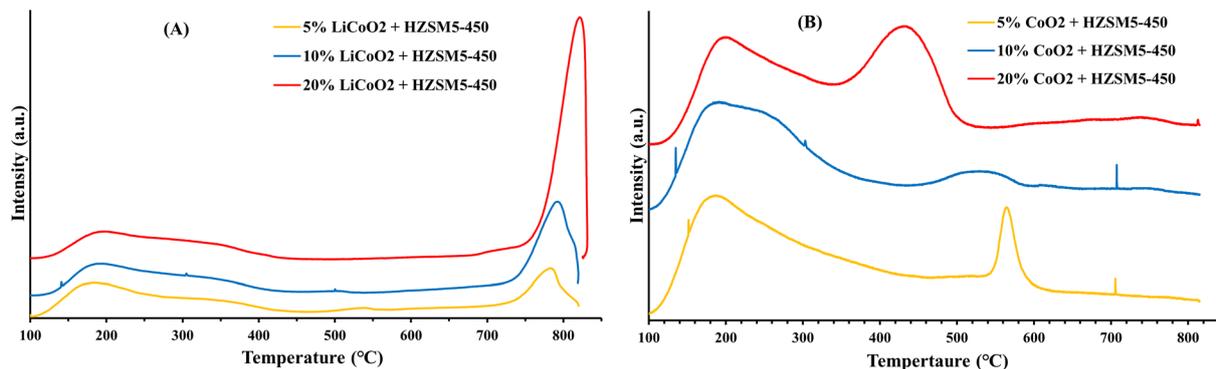
Fig. 4 NH$_3$-TPD profiles of all the synthesized (A) LiCoO$_2$ and (B) Co$_3$O$_4$ loaded HZSM-5 catalysts.

Table 2 Acidity of all the synthesized LiCoO$_2$ and Co$_3$O$_4$ loaded HZSM-5 catalysts

| Catalysts | Acidity (mmolNH$_3$ g^{-1} cat) | | | |
	Weak acid <300 °C	Moderate acid 300–525 °C	Strong acid >525 °C	Total acidity
HZSM5	0.721	—	0.283	1.004
5% Co (LiCoO$_2$)/HZSM-5	0.578	—	0.483	1.061
10% Co (LiCoO$_2$)/HZSM-5	0.519	—	0.625	1.144
20% Co (LiCoO$_2$)/HZSM-5	0.508	—	1.118	1.626
5% Co (Co$_3$O$_4$)/HZSM-5	0.717	—	0.315	1.032
10% Co (Co$_3$O$_4$)/HZSM-5	0.574	—	0.308	0.882
20% Co (Co$_3$O$_4$)/HZSM-5	0.373	0.368	0.208	0.949

acidity of LiCoO$_2$/HZSM-5. The catalytic decomposition of NH$_3$ was assigned to the distinct desorption peak at ∼550 °C for 5% Co (Co$_3$O$_4$)/HZSM-5. This peak shifted to a lower temperature with an increase in the cobalt content of the catalyst (Fig. 4B). For LiCoO$_2$-impregnated HZSM-5 catalysts, the high-intensity peak between 750 and 800 °C was ascribed to the reduction of Li$^+$ to Li metal.[42]

3.1.5 FESEM and ICP-OES analysis. Fig. 5 shows the FESEM micrographs of LiCoO$_2$ and Co$_3$O$_4$-loaded HZSM5 catalysts. Although the orthogonal-shaped HZSM-5 crystals are seen loaded with the agglomerates of LiCoO$_2$ and Co$_3$O$_4$ particles, the decrease in BET surface area and total pore volume with an increase in cobalt content suggests the deposition of

LiCoO$_2$ and Co$_3$O$_4$ in the pores of the HZSM-5 support (Table 1). Lithium and cobalt contents of the synthesized catalysts were determined by ICP-OES analysis following the aqua regia method. Table S1 (ESI†) lists the actual contents of lithium and cobalt in all the synthesized catalysts. Lithium and cobalt contents were a little lower than the calculated values. This was attributed to the formation of surface hydroxyls and sample humidity before and after impregnation.

3.1.6 FTIR analysis. Fig. S2 (ESI†) shows the FTIR absorption spectra of all Co$_3$O$_4$/HZSM5 catalysts. The two absorption bands at 546 and 665 cm^{-1} relate to the stretching vibration of the cobalt–oxygen bond in the Co$_3$O$_4$ spinel lattice.[43] The stretching vibration bands at 546 cm^{-1} and 665 cm^{-1} were assigned to the octahedrally coordinated Co^{3+} and tetrahedrally coordinated Co^{2+} with oxygen, respectively.[44] The peak intensity of tetrahedrally coordinated Co^{2+} with oxygen (Co^{2+}– O) increased with an increase in the weight percentage of cobalt in the catalysts while the peak intensity of tetrahedrally coordinated Co^{3+} remained unchanged. For LiCoO$_2$/HZSM-5 catalysts, no change in the stretching vibrations was observed upon increasing the weight percentage content of Co in the catalyst (Fig. S3, ESI†).

3.2 Upgrading of stock bio-oil

The upgraded bio-oils obtained upon catalytic treatment of stock bio-oils with LiCoO$_2$ and Co$_3$O$_4$ impregnated hierarchical nano-ZSM-5 showed substantial differences in the chemical

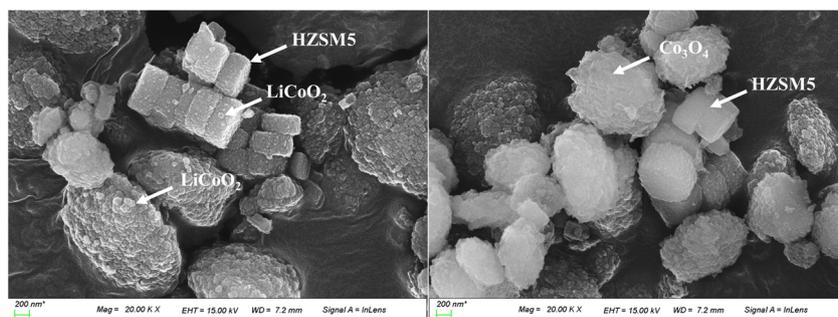**Fig. 5** FESEM micrographs of LiCoO$_2$ and Co$_3$O$_4$ loaded HZSM-5 catalysts.

Table 3 Yields of major compounds (by relative % peak area) obtained upon bio-oil upgrading over all the synthesized $LiCoO_2$ and Co_3O_4 loaded HZSM-5 catalysts

Compounds	Stock bio-oil	No catalyst	HZSM-5	5% Co ($LiCoO_2$)/ HZSM-5	10% Co ($LiCoO_2$)/ HZSM-5	20% Co ($LiCoO_2$)/ HZSM-5	5% Co (Co_3O_4)/ HZSM-5	10% Co (Co_3O_4)/ HZSM-5	20% Co (Co_3O_4)/ HZSM-5
Guaiacol	**12.4**	**11.6**	**11.3**	**10.3**	**10.5**	**10.3**	**10.7**	**9.9**	**10.1**
4-Methylguaiacol	10.2	10.7	10.9	13.1	13.0	10.5	12.9	11.7	10.7
4-Ethylguaiacol	13.5	14.2	14.8	15.1	15.5	13.4	15.1	13.8	13.1
4-Propylguaiacol	9.0	12.8	13.6	16.4	17.1	14.0	15.4	15.5	14.6
Total	**32.7**	**37.7**	**39.3**	**44.6**	**45.6**	**37.9**	**43.4**	**41.0**	**38.4**
4-(1-Propenyl)guaiacol	7.0	3.6	3.5	2.1	2.6	1.5	3.4	2.8	2.4
Homovanillyl alcohol	4.7	3.8	3.8	4.5	4.6	2.8	6.2	6.1	5.1
Ethyl vanillate	1.2	—	—	—	—	—	1.8	—	1.7
Homovanillic acid	8.2	6.6	6.0	4.3	4.9	4.9	6.1	6.6	6.6
Methyl-(3-methoxy-4-hydroxy-benzyl)-ether	—	—	—	—	—	—	3.9	5.5	3.3
Dehydroabietic acid	2.2	4.6	3.9	9.4	9.4	7.4	4.5	5.4	7.2
Gibberellin	3.6	2.0	3.0	—	4.7	3.9	2.2	0.5	5.5
7,8-Dimethoxy-3,3-dimethyl-1-methylene-1,2,3,4-tetrahydrodibenzofuran	5.5	—	—	—	—	—	—	—	-

composition. The compounds in the upgraded bio-oils as detected by GC-MS analysis are listed in Table 3. Few compounds remained unidentified due to the chemical complexity of bio-oils and the restricted ability of GC-MS analysis.[45] The compounds in the upgraded bio-oils were recognized by fitting the obtained GC-MS spectra with the National Institute of standards and Technology (NIST) mass spectral library. The variations in the resultant peak areas of the upgraded bio-oils were used to determine changes in the yields of compounds.[46] Authentic reference compounds were used to compare these variations. The stock bio-oil was characterized *via* the presence of guaiacols (~52.1%), homovanillic acid (~8.2%), homovanillyl alcohol (~4.7%), 7,8-dimethoxy-3,3-dimethyl-1-methylene-1,2,3,4-tetrahydrodibenzofuran (~5.5%) and gibberellin (~3.6%). Alkylated guaiacols were the key compounds that accounted for ~32.7% of the total compounds that were present in the stock bio-oil obtained upon liquefaction of Kraft lignin in supercritical ethanol. Upon bio-oil upgrading, alkylated guaiacols (4-methylguaiacol, 4-ethylguaiacol, and 4-propylguaiacol) and dehydroabietic acid enhanced substantially while guaiacol, 4-(1-propenyl) guaiacol and homovanillic acid reduced over all the catalysts.

Despite having a slightly smaller BET surface area than the corresponding Co_3O_4/HZSM-5 catalysts, $LiCoO_2$/HZSM-5 with low cobalt content (5% and 10% Co) showed high selectivity for the production of alkylated guaiacols owing to their strong acidity in comparison with Co_3O_4/HZSM-5 catalysts. This suggests that at low cobalt content, the effect of strong acidity was more significant than the BET surface area of the catalysts in regulating the percentage of total alkylated guaiacols. On the other hand, although the total acidity of 20% Co ($LiCoO_2$)/HZSM-5 was considerably higher than that of 20% Co (Co_3O_4)/HZSM-5, the relative percentage of total alkylated guaiacols obtained was low for the former due to the appreciably small BET surface area than the latter. It was inferred that the roles of strong acidity and BET surface area in governing the catalytic activity of the synthesized catalysts were more prominent

at low and high cobalt contents, respectively. Besides this, lithium played a major role in promoting the alkylation of guaiacols by favoring the cleavage of C–H bonds followed by the subsequent formation of C–C bonds. This resulted in an increase in the total yield of alkylated guaiacols for $LiCoO_2$/HZSM-5 catalysts. Recently, low concentration of lithium has been found to promote the weakening of the C–H bond during the water–gas shift reaction while at high concentration the trend reversal occurred.[47] In addition, lately, lithium has also been found to play a significant role in fostering C–C bond formation *via* an electron capture-based mechanism.[48] Apart from alkylated guaiacols, a considerable increase in the amount of dehydroabietic acid was also observed for upgraded bio-oil obtained over $LiCoO_2$/HZSM-5 compared to Co_3O_4/HZSM-5 catalysts. Dehydroabietic acid is an important aromatic compound that finds application in the synthesis of surfactants, antioxidants, and chiral catalysts.[49] Besides, it also has potential as a treatment for obesity and metabolic syndrome.[50] In addition, homovanillyl alcohol which is often applied for the prevention of cardiovascular disease[51] was present in higher amounts in the upgraded bio-oil acquired over Co_3O_4/HZSM-5 compared to $LiCoO_2$/HZSM-5 catalysts. Although several cobalt-based catalysts such as Co/SiO_2, Co/HZSM5, $Fe-Co/SiO_2$,[52] $Co-Mo/Al_2O_3$,[53] Co–Zn/HZSM5,[40] and $Co-Mo/MCM-41$[54] have shown significant improvement in upgrading the quality of bio-oil in supercritical fluids, the high cost of cobalt often raises concern regarding the industrial use of this metal as a catalyst for bio-oil upgrading. As an alternative, $LiCoO_2$ obtained from the cathode material of spent LIBs appears as a cheaper alternative to be used as an efficient catalyst for bio-oil upgrading besides simultaneously addressing the e-waste management issue in a sustainable manner leading to a win–win situation.

Fig. 6 shows the plausible reaction pathways for bio-oil upgrading. Alkylation, deoxygenation, and hydrogenation were the key mechanisms responsible for the formation of distinct monomers upon bio-oil upgrading. Cobalt has been widely
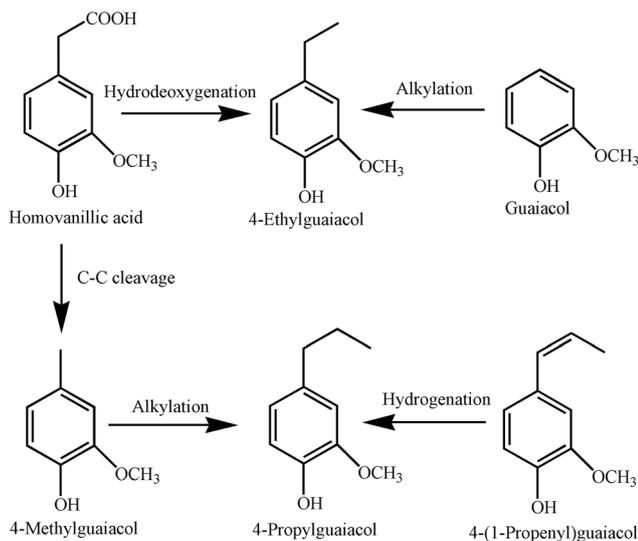
Fig. 6 Plausible reaction pathways for the formation of different monomers.

Fig. 7 Van Krevelen diagram for stock and upgraded bio-oils obtained over all the synthesized $LiCoO_2$ and Co_3O_4 loaded HZSM-5 catalysts.

studied for HDO of phenolic compounds.[9] Compared with other transition metals, cobalt exhibits better catalytic performance due to its high efficacy for removing oxygen by direct deoxygenation.[55,56] Additionally, during solvothermolysis of lignin, ethanol behaves as a hydrogen donor that enables the creation of alkylated guaiacols.[57] In this study, a noteworthy increase in the quantity of 4-propylguaiacol (Table 3) was ascribed to the alkylation and hydrogenation of 4-methylguaiacol and 4-(1-propenylguaiacol), respectively while the HDO and alkylation of homovanillic acid and guaiacol, respectively, resulted in the formation of 4-ethylguaiacol. The total alkylated guaiacols increased from 32.7% for the stock bio-oil to 45.6% for upgraded bio-oil obtained over the 10% Co $(LiCoO_2)$/HZSM-5 catalyst. In contrast, for Co_3O_4 impregnated HZSM-5 catalysts, the total alkylated guaiacols increased only to a maximum of 43.4% over 5% Co (Co_3O_4)/HZSM-5.

Table 4 lists the elemental compositions of the bio-oils obtained over all the synthesized catalysts. From Fig. 7 (Van Krevelen diagram) it is clear that the highest atomic H/C ratio (1.286) and the lowest atomic O/C ratio (0.262) were attained for the 10% Co $(LiCoO_2)$/HZSM-5 catalyst. Both hydrogenation
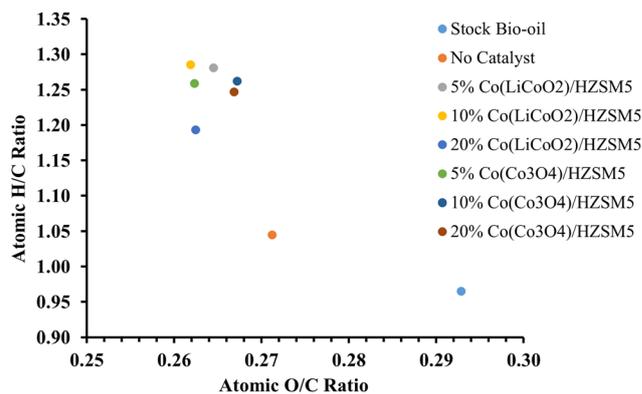
and deoxygenation were prominent for this catalyst resulting in a maximum increase in HHV from 27.03 MJ kg^{-1} (stock bio-oil) to 29.83 MJ kg^{-1} for the upgraded bio-oil. HHV is the amount of energy released upon combustion of 1 g of fuel to generate CO_2 and H_2O at its initial temperature and pressure. Since a high HHV denotes a good quality fuel, the increase in HHV from 27.03 MJ kg^{-1} (stock bio-oil) to 29.83 MJ kg^{-1} for the upgraded bio-oil confirms the formation of better quality biofuel. Over the 10% Co $(LiCoO_2)$/HZSM-5 catalyst, the percentage of hydrogen in the upgraded bio-oil increased up to 7.30% while the percentage of oxygen decreased to a minimum of 23.80% in comparison with all other catalysts. The sulfur content also showed a significant decrease from 0.78% (stock bio-oil) to 0.43% for the upgraded bio-oil obtained over the 10% Co $(LiCoO_2)$/HZSM-5 catalyst.

3.3 Spent catalyst characterization and stability

Fig. 8 shows the TG and derivative TG plots of fresh and spent 10% Co $(LiCoO_2)$/HZSM5 catalysts. The spent catalyst showed a significant weight loss of ~48% compared to the original catalyst with the maximum weight loss occurring at 430 °C. This weight loss was attributed to the combustion of coke deposited on the catalyst. The XRD pattern (Fig. 9) revealed a noteworthy change in the chemical composition of the spent catalysts obtained after cycles I and II compared to the fresh catalyst. A substantial change in the intensity and position of the diffrac-

Table 4 Elemental analysis and HHV (MJ kg^{-1}) values of stock and upgraded bio-oils obtained over all the synthesized $LiCoO_2$ and Co_3O_4 loaded HZSM-5 catalysts

| Sample	N (%)	C (%)	H (%)	S (%)	O (%)	Atomic ratios		HHV$_{Boie}$ (MJ kg^{-1})
						O/C	H/C	
Stock Bio-oil	0.45	67.15	5.40	0.78	26.22	0.293	0.965	27.03
No Catalyst	0.43	68.19	5.94	0.78	24.66	0.271	1.045	28.20
5% Co($LiCoO_2$)/HZSM-5	0.41	67.92	7.25	0.47	23.95	0.265	1.281	29.67
10% Co($LiCoO_2$)/HZSM-5	0.33	68.14	7.30	0.43	23.80	0.262	1.286	29.83
20% Co($LiCoO_2$)/HZSM-5	0.54	68.32	6.79	0.44	23.91	0.262	1.193	29.28
5% Co(Co_3O_4)/HZSM-5	0.41	68.10	7.15	0.53	23.82	0.262	1.259	29.64
10% Co(Co_3O_4)/HZSM-5	0.45	67.80	7.13	0.47	24.16	0.267	1.263	29.47
20% Co(Co_3O_4)/HZSM-5	0.46	67.87	7.06	0.46	24.15	0.267	1.247	29.41
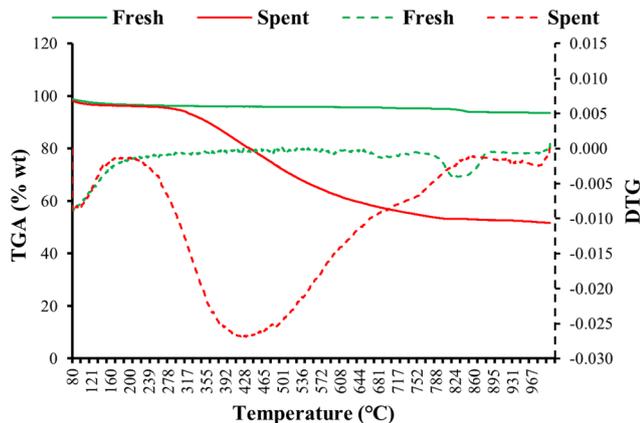
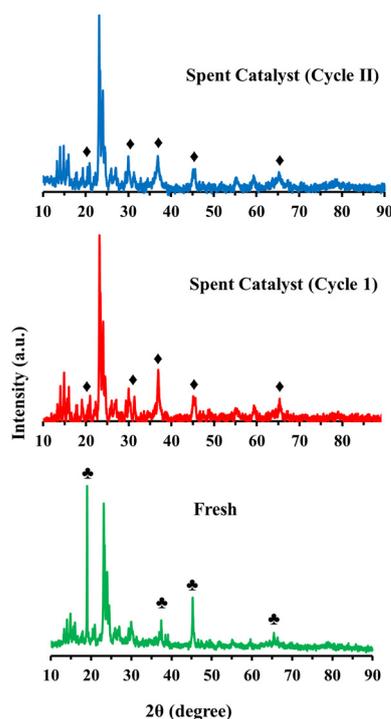**Fig. 8** TG and derivative TG plots of fresh and spent 10% Co (LiCoO₂)/HZSM-5 catalysts (cycle I).

Fig. 9 XRD patterns of fresh and spent 10% Co (LiCoO₂)/HZSM-5 catalysts (cycle I & II).

tion peaks corresponding to LiCoO₂ was observed, while the triplet between $2\theta = 22°$–$25°$ in the XRD diffractograms showed that the characteristic MFI structure of HZSM5 remained almost undamaged. For the spent catalysts the disappearance of a strong diffraction peak at $2\theta = 18.99°$ suggested a complete loss of lithium from the catalysts. This was reaffirmed by ICP-OES analysis. In addition, the diffraction peak intensity pattern of the spent catalysts at $2\theta = 19.0°$, $31.3°$, $36.5°$, $44.8°$, $65.2°$ matched completely with that of Co₃O₄ indicating the formation of Co₃O₄ upon loss of lithium from the catalyst.

Since the HHV of upgraded bio-oil (Table 4) obtained over Co₃O₄ loaded HZSM5 catalysts is low compared to that over 10% LiCoO₂ loaded HZSM5, the overall performance of the spent catalyst acquired upon the loss of lithium will be lower than that of the original catalyst. Although the 10% Co (LiCoO₂)/HZSM5 catalyst enhanced the HHV of bio-oil, the complete loss of lithium from the catalyst raises concerns regarding contamination of the upgraded bio-oil. Future research is, therefore, essential to avoid the possible release of lithium from the catalyst and to maintain its catalytic properties. Furthermore, the peak position and intensity of the spent catalyst (cycle II) were almost identical to that of the spent catalyst obtained after the first round of bio-oil upgrading (cycle I). This suggests that the crystal structure of the spent catalyst (cycle I) remained intact even after the second round (cycle II) of bio-oil upgrading.

4. Conclusions

Upgrading of liquefaction bio-oil over LiCoO₂ and Co₃O₄ impregnated HZSM-5 catalysts significantly enhanced the amounts of alkylated guaiacols by reducing the amounts of unsubstituted guaiacols, alkenyl guaiacols, and homovanillic acid. Alkylation, deoxygenation, and hydrogenation were the plausible bio-oil upgrading pathways. Among all the synthesized catalysts, the maximum HHV$_{\text{Boie}}$ (~29.83 MJ kg^{-1}) was attained over 10% Co (LiCoO₂)/HZSM-5. Catalytic upgrading not only reduced the oxygen percentage, but also enhanced the carbon and hydrogen contents of the bio-oils. Structural characterization of the spent catalyst suggested a complete loss of lithium from the catalyst resulting in the formation of Co₃O₄, while the MFI framework of the HZSM-5 support remained intact. It was demonstrated in this study that the main constituent of the cathode material of spent LIBs *i.e.* LiCoO₂ can be employed to synthesize a cheap and novel catalyst for bio-oil upgrading. It is expected that this study will open a new window for the reuse of spent LIBs (e-waste) as the cheapest source of valuable metals for catalytic production and upgrading of bio-oil. This may lead to a sustainable approach for future e-waste management.

Author contributions

Ashutosh Agarwal: conceptualization, methodology, software, formal analysis, investigation, writing – original draft, and writing – review and editing. Xue Li: investigation, validation, visualization, and writing – review and editing.

Conflicts of interest

The authors declare no conflict of interest.

Acknowledgements

References

1 A. Agarwal, M. Rana and J.-H. Park, *Fuel Process. Technol.*, 2018, **181**, 115–132.

2 Z. Al-Hamamre, M. Saidan, M. Hararah, K. Rawajfeh, H. E. Alkhasawneh and M. Al-Shannag, *Renewable Sustainable Energy Rev.*, 2017, **67**, 295–314.

3 S. S. Wong, R. Shu, J. Zhang, H. Liu and N. Yan, *Chem. Soc. Rev.*, 2020, **49**, 5510–5560.

4 S. Xiu and A. Shahbazi, *Renewable Sustainable Energy Rev.*, 2012, **16**, 4406–4414.

5 P. J. Deuss, M. Scott, F. Tran, N. J. Westwood, J. G. de Vries and K. Barta, *J. Am. Chem. Soc.*, 2015, **137**, 7456–7467.

6 M. Bartoli, L. Rosi, P. Frediani and M. Frediani, *Fuel*, 2020, **278**, 118175–118184.

7 S. Kadarwati, X. Hu, R. Gunawan, R. Westerhof, M. Gholizadeh, M. D. M. Hasan and C.-Z. Li, *Fuel Process. Technol.*, 2017, **155**, 261–268.

8 A. Ramesh, P. Tamizhdurai and K. Shanthi, *Renewable Energy*, 2019, **138**, 161–173.

9 W. Jin, L. Pastor-Pérez, D. Shen, A. Sepúlveda-Escribano, S. Gu and T. R. Reina, *ChemCatChem*, 2019, **11**, 924–960.

10 V. M. L. Whiffen and K. J. Smith, *Energy Fuels*, 2010, **24**, 4728–4737.

11 Z. Ma, L. Wei, W. Zhou, L. Jia, B. Hou, D. Li and Y. Zhao, *RSC Adv.*, 2015, **5**, 88287–88297.

12 Y. Yang, L. Qiao, J. Hao, H. Shi and G. Lv, *Chem. Eng. Sci.*, 2019, **208**, 115154–115160.

13 M. Saidi, H. R. Rahimpour, B. Rahzani, P. Rostami, B. C. Gates and M. R. Rahimpour, *Can. J. Chem. Eng.*, 2016, **94**, 1524–1532.

14 A. Agarwal, S.-J. Park and J.-H. Park, *Ind. Eng. Chem. Res.*, 2019, **58**, 22791–22803.

15 X. Dou, X. Jiang, W. Li, C. Zhu, Q. Liu, Q. Lu, X. Zheng, H.-m. Chang and H. Jameel, *Appl. Catal., B*, 2020, **268**, 118429–118445.

16 A. Bakhtyari, M. R. Rahimpour and S. Raeissi, *Renewable Energy*, 2020, **150**, 443–455.

17 N. T. T. Tran, Y. Uemura, A. Ramli and T. H. Trinh, *Mol. Catal.*, 2022, **523**, 111435.

18 W. Moonsrikaew and A. Duangchan, *Mol. Catal.*, 2022, **523**, 111712.

19 Z. Ma, V. Custodis and J. A. van Bokhoven, *Catal. Sci. Technol.*, 2014, **4**, 766–772.

20 X. Liu, L. Xu, G. Xu, W. Jia, Y. Ma and Y. Zhang, *ACS Catal.*, 2016, **6**, 7611–7620.

21 E. Rodríguez-Aguado, A. Infantes-Molina, J. A. Cecilia, D. Ballesteros-Plata, R. López-Olmo and E. Rodríguez-Castellón, *Top. Catal.*, 2017, **60**, 1094–1107.

22 D. Raikwar, S. Majumdar and D. Shee, *Mol. Catal.*, 2021, **499**, 111290–111304.

23 B. Qiu, C. Yang, Q. Shao, Y. Liu and H. Chu, *Fuel*, 2022, **315**, 123218.

24 A. Chitre, D. Freake, L. Lander, J. Edge and M.-M. Titirici, *Batteries Supercaps*, 2020, **3**, 1126–1136.

25 T. Liu, S. Cai, G. Zhao, Z. Gao, S. Liu, H. Li, L. Chen, M. Li, X. Yang and H. Guo, *J. Energy Chem.*, 2021, **62**, 440–450.

26 M. Guo, X. Wang, L. Liu, X. Min, X. Hu, W. Guo, N. Zhu, J. Jia, T. Sun and K. Li, *Environ. Res.*, 2021, **193**, 110563.

27 L. Chen, P. Wang, Y. Shen and M. Guo, *Bioresour. Technol.*, 2021, **323**, 124584.

28 P. Wang, L. Chen and Y. Shen, *Bioresour. Technol.*, 2021, **337**, 125476.

29 X. Zhu, Z. Shi, X. Zhu, Y. Lai, J. Ma, A. Xia, Y. Huang and Q. Liao, *Fuel*, 2022, **326**, 125018.

30 Y. Shen, *J. Power Sources*, 2022, **528**, 231220.

31 A. Veses, B. Puértolas, J. M. López, M. S. Callén, B. Solsona and T. García, *ACS Sustainable Chem. Eng.*, 2016, **4**, 1653–1660.

32 T. Nshizirungu, A. Agarwal, Y. T. Jo, M. Rana, D. Shin and J.-H. Park, *J. Hazard. Mater.*, 2020, **393**, 122367–122373.

33 K. Liu and F.-S. Zhang, *J. Hazard. Mater.*, 2016, **316**, 19–25.

34 A. A. Rownaghi, F. Rezaei and J. Hedlund, *Microporous Mesoporous Mater.*, 2012, **151**, 26–33.

35 K. Annamalai, J. M. Sweeten and S. C. Ramalingam, *Trans. ASAE*, 1987, **30**, 1205–1208.

36 C. Julien, *Solid State Ionics*, 2003, **157**, 57–71.

37 E. Antolini and M. Ferretti, *J. Solid State Chem.*, 1995, **117**, 1–7.

38 K. Ding, Z. Zhong, J. Wang, B. Zhang, M. Addy and R. Ruan, *J. Anal. Appl. Pyrolysis*, 2017, **125**, 153–161.

39 L. Dahéron, H. Martinez, R. Dedryvère, I. Baraille, M. Ménétrier, C. Denage, C. Delmas and D. Gonbeau, *J. Phys. Chem. C*, 2009, **113**, 5843–5852.

40 S. Cheng, L. Wei, J. Julson, K. Muthukumarappan and P. R. Kharel, *Energy Convers. Manage.*, 2017, **147**, 19–28.

41 G. Ramis, L. Yi, G. Busca, M. Turco, E. Kotur and R. J. Willey, *J. Catal.*, 1995, **157**, 523–535.

42 T. Dai, H. Zhou, Y. Liu, R. Cao, J. Zhan, L. Liu and B. W. L. Jang, *ACS Sustainable Chem. Eng.*, 2019, **7**, 5072–5081.

43 Z. Zhu, G. Lu, Z. Zhang, Y. Guo, Y. Guo and Y. Wang, *ACS Catal.*, 2013, **3**, 1154–1164.

44 M. Salavati-Niasari, N. Mir and F. Davar, *J. Phys. Chem. Solids*, 2009, **70**, 847–852.

45 H. Ben and A. J. Ragauskas, *Energy Fuels*, 2011, **25**, 4662–4668.

46 Q. Lu, Z.-F. Zhang, C.-Q. Dong and X.-F. Zhu, *Energies*, 2010, **3**, 1805–1820.

47 Z. Rajabi, M. Martinelli, C. D. Watson, D. C. Cronauer, A. Jeremy Kropf and G. Jacobs, *Int. J. Hydrogen Energy*, 2022, **47**, 30872–30895.

48 H. Tachikawa, *ACS Omega*, 2023, **8**, 10600–10606.

49 L. Lei, D. Xie, B. Song, J. Jiang, X. Pei and Z. Cui, *Langmuir*, 2017, **33**, 7908–7916.

50 M. S. Kang, S. Hirai, T. Goto, K. Kuroyanagi, Y. I. Kim, K. Ohyama, T. Uemura, J. Y. Lee, T. Sakamoto, Y. Ezaki, R. Yu, N. Takahashi and T. Kawada, *BioFactors*, 2009, **35**, 442–448.

51 R. De la Torre, D. Corella, O. Castañer, M. A. Martínez-González, J. Salas-Salvador, J. Vila, R. Estruch, J. V. Sorli, F. Arós, M. Fiol, E. Ros, L. Serra-Majem, X. Pintó, E. Gómez-Gracia, J. Lapetra, M. Ruiz-Canela, J. Basora, E. M. Asensio, M. I. Covas and M. Fitó, *Am. J. Clin. Nutr.*, 2017, **105**, 1297–1304.

52 S. Cheng, L. Wei, J. Julson and M. Rabnawaz, *Energy Convers. Manage.*, 2017, **150**, 331–342.

53 C. Muangsuwan, W. Kriprasertkul, S. Ratchahat, C. G. Liu, P. Posoknistakul, N. Laosiripojana and C. Sakdaronnarong, *ACS Omega*, 2021, **6**, 2999–3016.

54 S. Taghavi, E. Ghedini, F. Menegazzo, M. Signoretto, D. Gazzoli, D. Pietrogiacomi, A. Matayeva, A. Fasolini, A. Vaccari, F. Basile and G. Fornasari, *Processes*, 2020, **8**(843), 1–15.

55 Y. Yang, G. Lv, L. Deng, B. Lu, J. Li, J. Zhang, J. Shi and S. Du, *Microporous Mesoporous Mater.*, 2017, **250**, 47–54.

56 T. Mochizuki, S.-Y. Chen, M. Toba and Y. Yoshimura, *Appl. Catal., B*, 2014, **146**, 237–243.

57 H.-s. Lee, J. Jae, J.-M. Ha and D. J. Suh, *Bioresour. Technol.*, 2016, **203**, 142–149.